

# On the applicability of density dependent effective interactions in cluster-forming systems

Marta Montes-Saralegui, Gerhard Kahl, and Arash Nikoubashman

Citation: *The Journal of Chemical Physics* **146**, 054904 (2017); doi: 10.1063/1.4975164

View online: <https://doi.org/10.1063/1.4975164>

View Table of Contents: <http://aip.scitation.org/toc/jcp/146/5>

Published by the [American Institute of Physics](#)

---

## Articles you may be interested in

[Perspective: Dissipative particle dynamics](#)

*The Journal of Chemical Physics* **146**, 150901 (2017); 10.1063/1.4979514

[Dynamics of single semiflexible polymers in dilute solution](#)

*The Journal of Chemical Physics* **145**, 234903 (2016); 10.1063/1.4971861

[Coarse-grained models using local-density potentials optimized with the relative entropy: Application to implicit solvation](#)

*The Journal of Chemical Physics* **145**, 034109 (2016); 10.1063/1.4958629

[On the representability problem and the physical meaning of coarse-grained models](#)

*The Journal of Chemical Physics* **145**, 044108 (2016); 10.1063/1.4959168

[Bottom-up coarse-grained models that accurately describe the structure, pressure, and compressibility of molecular liquids](#)

*The Journal of Chemical Physics* **143**, 243148 (2015); 10.1063/1.4937383

[Extending the range and physical accuracy of coarse-grained models: Order parameter dependent interactions](#)

*The Journal of Chemical Physics* **147**, 044113 (2017); 10.1063/1.4995946

---

PHYSICS TODAY

WHITEPAPERS

### ADVANCED LIGHT CURE ADHESIVES

Take a closer look at what these environmentally friendly adhesive systems can do

READ NOW

PRESENTED BY  
 MASTERBOND  
ADHESIVES | SEALANTS | COATINGS

# On the applicability of density dependent effective interactions in cluster-forming systems

Marta Montes-Saralegui,<sup>1</sup> Gerhard Kahl,<sup>1</sup> and Arash Nikoubashman<sup>2,a)</sup>

<sup>1</sup>*Institute for Theoretical Physics and Center for Computational Material Science (CMS), Technische Universität Wien, Wiedner Hauptstraße 8-10, A-1040 Wien, Austria*

<sup>2</sup>*Institute of Physics, Johannes Gutenberg University Mainz, Staudingerweg 7, 55128 Mainz, Germany*

(Received 23 September 2016; accepted 18 January 2017; published online 7 February 2017)

We systematically studied the validity and transferability of the force-matching algorithm for computing effective pair potentials in a system of dendritic polymers, i.e., a particular class of ultrasoft colloids. We focused on amphiphilic dendrimers, macromolecules which can aggregate into clusters of overlapping particles to minimize the contact area with the surrounding implicit solvent. Simulations were performed for both the monomeric and coarse-grained models in the liquid phase at densities ranging from infinite dilution up to values close to the freezing point. The effective pair potentials for the coarse-grained simulations were computed from the monomeric simulations both in the zero-density limit ( $\Phi_{\text{eff}}^0$ ) and at each investigated *finite* density ( $\Phi_{\text{eff}}$ ). Conducting the coarse-grained simulations with  $\Phi_{\text{eff}}^0$  at higher densities is not appropriate as they failed at reproducing the structural properties of the monomeric simulations. In contrast, we found excellent agreement between the spatial dendrimer distributions obtained from the coarse-grained simulations with  $\Phi_{\text{eff}}$  and the microscopically detailed simulations at low densities, where the macromolecules were distributed homogeneously in the system. However, the reliability of the coarse-grained simulations deteriorated significantly as the density was increased further and the cluster occupation became more polydisperse. Under these conditions, the effective pair potential of the coarse-grained model can no longer be computed by averaging over the whole system, but the local density needs to be taken into account instead. *Published by AIP Publishing.* [<http://dx.doi.org/10.1063/1.4975164>]

## I. INTRODUCTION

Amphiphiles are chemical compounds consisting of both solvophilic and solvophobic blocks. When the solute concentration surpasses a certain threshold, these particles spontaneously self-assemble into micellar aggregates to minimize the interface between the solvophobic block and the surrounding solvent. The size and shape of the self-assembled superstructures depend mainly on the microscopic properties of the amphiphiles, allowing for, e.g., spherical, cylindrical, and lamellar aggregates.<sup>1</sup> This peculiar ability makes amphiphilic molecules indispensable for a wide variety of applications,<sup>2-4</sup> for example, as cleaning agents or emulsifiers in the cosmetic and food industry.

In this work, we focus on the self-assembly behavior of amphiphilic dendrimers, which consist of a solvophobic core and a solvophilic shell. Recently, these macromolecules have gathered an increasing amount of attention due to their propensity to form long-lived colloidal crystals, where each lattice site is populated by an aggregate.<sup>5-15</sup> Simulation studies of these so-called cluster crystals have revealed a wide range of peculiar static and dynamic properties, which sets them apart from conventional single occupancy crystals. For example, the lattice constant of the cluster crystals is density-independent, and therefore external pressure does not lead to a compression of the lattice but rather to an increase of the occupation

number.<sup>15</sup> The dynamics of this process are characterized by activated hopping of the constituent particles and merging of neighboring lattice sites.<sup>7,9,13-15</sup> Furthermore, reentrant melting and isostructural phase transitions have been reported for this class of amphiphiles.<sup>8,10</sup>

Due to computational limitations, the majority of previous simulation studies relied on coarse-grained (CG) models, where the macromolecular amphiphiles were modeled as single interaction sites. The corresponding effective pair interactions were usually obtained in the limit of infinite dilution and have then been employed to calculate system properties at considerably higher densities.<sup>6,8</sup> However, this strategy might lead to an inaccurate representation of the original microscopic model, since the transferability of the effective pair potentials from infinite dilution to finite densities is *a priori* not obvious.<sup>16</sup> For instance, it has been demonstrated for homopolymer systems that additional corrections are necessary to provide a faithful CG representation of the microscopically resolved (MR) systems at finite densities.<sup>17</sup>

To shed more light on this question, we performed a systematic analysis of amphiphilic dendrimers in the liquid phase at densities ranging from infinite dilution up to close to the freezing point. We computed the effective potentials at each state point using a force-matching CG algorithm.<sup>18-22</sup> We then compared the emerging structures in the MR and CG simulations using the effective (pair) potentials obtained at infinite dilution,  $\Phi_{\text{eff}}^0$ , and at the corresponding density,  $\Phi_{\text{eff}}$ . We discovered that the CG simulations with  $\Phi_{\text{eff}}^0$  failed at reproducing

<sup>a)</sup>Electronic mail: anikouba@uni-mainz.de

the MR structures even at the lowest investigated densities, and significantly underestimated the freezing density. The CG simulations with  $\Phi_{\text{eff}}$  exhibited good agreement with the microscopic reference simulations at low densities, where the system predominantly consisted of isolated amphiphiles and small clusters. However, the agreement deteriorated rapidly as the density was increased further.

We did not expect such a significant deviation between the two representations because the effective potentials employed in the CG simulations were calculated from MR simulations conducted at exactly the *same* density and temperature. This discrepancy can be rationalized by considering the spatial density variations in the system, which became more pronounced as the amphiphiles started to aggregate into clusters of heterogeneous size. These inhomogeneities make it impossible to represent *all* relevant interactions by a *single* effective pair potential. To validate our hypothesis, we systematically calculated the effective potential between aggregates of different sizes and found a highly non-linear relationship between the effective interaction and the aggregation number.

The rest of this manuscript is organized as follows. In Section II A, we introduce the investigated model systems and simulation method. The employed CG algorithm is presented in Section II B. We discuss our findings in Section III, where we systematically compare our results from the microscopically resolved simulations with the coarse-grained ones. Finally, we summarize the findings and draw our conclusions in Section IV.

## II. MODELS AND METHODS

### A. Systems and simulation method

Dendrimers are characterized by a highly branched architecture, which is specified by the functionality,  $f$ , the spacer length,  $p$ , and the total number of generations,  $G$ . Dendrimers are grown by attaching  $(f - 1)$  chains with  $p$  monomers to two bonded central monomers (generation index  $g = 0$ ). This process was repeated  $G$  times, resulting in a self-similar structure. Figure 1 shows a schematic representation of the resulting dendritic macromolecule.

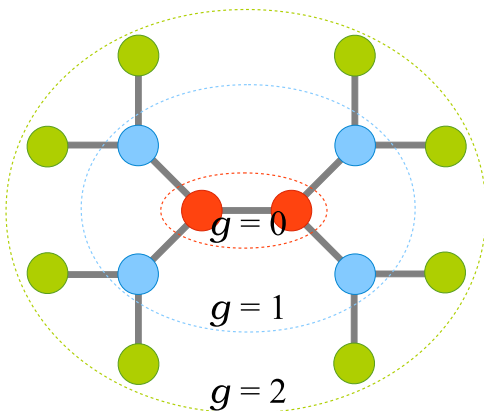


FIG. 1. Schematic representation of a dendrimer with parameters  $f = 3$ ,  $p = 1$ , and  $G = 2$  (see text). Each shell of the monomers is specified by its respective generation index  $g$ . Inner core monomers are colored in red and blue, while the outer shell monomers are shown in green.

All MR simulations were conducted using a bead-spring model, where the constituent monomers were represented by spherical beads with diameter  $\sigma$  that were tethered through massless springs. Three different cases were considered in this work: one non-clustering dendrimer model under good solvent conditions<sup>23</sup> and two different amphiphilic dendrimer models,<sup>6,12</sup> denoted henceforward by I and II. An implicit solvent model was used in all simulations, where we characterized the solvophilicity and solvophobicity of the monomers through their mutual pair interactions (see Table I).

In all three cases, the dendrimers are specified by  $f = 3$ ,  $p = 1$ , and  $G = 2$ , consisting thus of  $n_m = 14$  monomers. Furthermore, the mass of the beads was set to unity,  $m = 1$ . Covalent bonds were mimicked via the finite extensible non-linear elastic (FENE) potential,<sup>24,25</sup>

$$\beta\Phi^{\text{FENE}}(r_{ij}) = -\kappa_{ij}R_{ij}^2 \ln \left[ 1 - \left( \frac{r_{ij} - l_{ij}}{R_{ij}} \right)^2 \right], \quad (1)$$

with the reciprocal thermodynamic temperature of the system  $\beta = 1/(k_B T)$  and interparticle distance  $r_{ij} = |\mathbf{r}_j - \mathbf{r}_i|$ . The spring constant was controlled through the parameter  $\kappa_{ij}$ , whose magnitude depended on the identity of particles  $i$  and  $j$ . The minimum extension and maximum extension of the bond,  $l_{ij}^{\text{min}}$  and  $l_{ij}^{\text{max}}$ , respectively, were set through the parameters,

$$R_{ij} = (l_{ij}^{\text{max}} - l_{ij}) \quad \text{and} \quad l_{ij} = (l_{ij}^{\text{max}} + l_{ij}^{\text{min}})/2.$$

For the non-clustering dendrimers at good solvent conditions, all the beads had the same identity. Excluded volume interactions were modeled using the purely repulsive Weeks-Chandler-Andersen (WCA) potential,<sup>26</sup>

$$\beta\Phi^{\text{WCA}}(r_{ij}) = \begin{cases} 4\epsilon \left[ \left( \frac{\sigma}{r_{ij}} \right)^{12} - \left( \frac{\sigma}{r_{ij}} \right)^6 \right] + \epsilon & r_{ij} \leq 2^{1/6} \sigma \\ 0 & \text{otherwise,} \end{cases} \quad (2)$$

where the interaction strength is quantified through  $\epsilon$ .

In the case of the amphiphilic dendrimers, we distinguished between solvophobic core (C) and solvophilic shell (S) particles. Here, the bead-bead interactions were modeled via the Morse potential,

$$\beta\Phi^{\text{Morse}}(r_{ij}) = \epsilon_{ij} \left\{ \left[ e^{-\alpha_{ij}(r_{ij} - \sigma_{ij})} - 1 \right]^2 - 1 \right\}, \quad (3)$$

with  $\sigma_{ij} = (\sigma_i + \sigma_j)/2$ . The parameters  $\epsilon_{ij}$  and  $\alpha_{ij}$  controlled the strength and range of the interaction, respectively.

We used the interaction parameters from Ref. 23 for the non-clustering dendrimers at good solvent conditions and the interaction parameters from Ref. 6 (model I) and Ref. 12 (model II) for the amphiphilic dendrimers. The specific values are summarized in Table I. If not stated otherwise explicitly, we used in all our MR simulations  $\sigma = \sigma_{\text{CC}}$  as our unit of length, and  $m$  as our unit of mass. From these units, the intrinsic time unit of the MD simulations can be derived as  $\tau = \sigma \sqrt{\beta m}$ . Densities are defined as  $\rho = N/R_g$ , where  $N$  is the total number of dendrimers in the system and  $R_g$  is the radius of gyration of the dendrimers [see Eq. (5)]. The overlap density of the polymer solution,  $\rho_{\text{overlap}}$ , is defined as  $\frac{4}{3}\pi \left( \frac{3}{2}R_g \right)^3 \rho_{\text{overlap}} = 1$ .

TABLE I. Numerical parameters for the non-bonded (left) and bonded (right) interactions used in the MR simulations of non-clustering (NC) and amphiphilic dendrimers (model I and II). The abbreviations C and S refer to the different types of monomers involved in the respective interactions.

Model	Type	Interaction	$\epsilon_{ij}$	$\sigma_{ij}$	$\alpha_{ij}$	Type	Interaction	$\kappa_{ij}$	$l_{ij}$	$R_{ij}$
NC		WCA	1	1			FENE	0.5	0	10
I	CC	Morse	0.714	1	6.4	CC	FENE	40	1.875	0.375
	CS	Morse	0.014	1.25	19.2	CS	FENE	20	3.75	0.75
	SS	Morse	0.014	1.5	19.2					
II	CC	Morse	0.714	1	1.8	CC ( $g = 0$ )	FENE	60	3.1875	0.6375
	CS	Morse	0.017 85	1.75	6.0	CC ( $g \neq 0$ )	FENE	60	1.875	0.375
	SS	Morse	0.017 85	2.5	6.0	CS	FENE	30	3.5625	0.7125

Molecular dynamics simulations were conducted in the *NVT* ensemble using the LAMMPS simulation package.<sup>27</sup> The velocity Verlet algorithm<sup>28–30</sup> was employed for integrating the equations of motion, with a time step of  $\Delta t = 5 \times 10^{-4}$  for the MR simulations and  $\Delta t = 5 \times 10^{-3}$  for the CG simulations. In the CG simulations, we set the mass of the effective particles to unity, which introduced a factor of  $\sqrt{n_m} = \sqrt{14}$  between the time units in the MR and the CG picture.

The temperature was fixed to  $T = 1$  through a Nosé-Hoover thermostat.<sup>31–34</sup> The central idea of this scheme is to couple the system to an (implicit) external heat reservoir through a fictitious spring, allowing for heating as well as for dissipation of excess heat. Here, the coupling strength can be tuned via the damping time of the spring,  $t_d$ . On the one hand, too large values of  $t_d$  (loose coupling) may cause poor temperature control, whereas on the other hand, too small values (tight coupling) may cause high-frequency temperature oscillations. We found that  $t_d = 0.09$  led to quick equilibration as well as good temperature stability and therefore used this value in all our simulations.

The initial configurations for the MR simulations were generated by growing each of the  $N$  dendrimers along a self-avoiding random walk in a cubic simulation box. The systems were initialized in a highly diluted state, where the individual dendrimers were essentially isolated from each other. From these states, the final starting configurations were created by slowly compressing the simulation box until the desired density was reached. Once the starting configurations were produced, the systems were equilibrated until the potential energy did not change anymore.

## B. Coarse-graining method

In many situations, microscopically resolved simulations are computationally unfeasible due to the vast number of interaction sites. Such microscopic simulations are further impeded by the relatively small time steps, which are required for capturing the dynamics of the particles. Fortunately, the microscopic details of the individual macromolecules are often only of minor interest and can therefore be suitably traced out for the sake of computational efficiency. The acceleration achieved through such a coarse-graining is twofold: first, the number of interaction sites is reduced dramatically through this procedure, which facilitates the force calculation and the integration of the equations of motion. Second, CG models exhibit inherently faster dynamics compared to their MR counterparts

since the fast internal degrees of freedom have been integrated out.<sup>35</sup>

Various techniques have been developed to map the complex interactions of the MR system onto effective pair potentials. The mapping from the MR to the CG picture is in general *not* unique but depends on which of the physical quantities from the original MR system should be conserved.<sup>16</sup> One common strategy for systematic coarse-graining are the so-called “inversion schemes,” which calculate, on the basis of liquid state closure relations, the effective pair potential that reproduces a given pair correlation function  $g(r)$ . Among these are, for example, the simple inversion of the low-density relation  $\mathcal{F}(r) = -k_B T \ln g(r)$  [ $\mathcal{F}(r)$  being the free energy], an improved iterative scheme based on this relation (notably realized in the iterative Boltzmann inversion scheme, see, for example, Refs. 36 and 37), or an iterative predictor-corrector scheme, based on the more accurate modified hypernetted chain closure relation.<sup>38,39</sup> The idea common to all these approaches is to take an averaged *mesoscopic* quantity, e.g.,  $g(r)$ , that specifies the structure of the system and to calculate a pair potential that—when implemented in a computer simulation—reproduces the given structural correlation function. Even though the uniqueness of these schemes can be proven rigorously,<sup>40</sup> this feature is not strictly guaranteed in a numerical implementation of these algorithms due to statistical variations in the data.

Alternatively, effective pair interactions can also be computed by mapping on a *microscopic* level the forces acting on the monomer-resolved entities onto fictitious coarse-grained interaction sites. In our investigations, we employed one of these methods, the so-called multi-scale coarse graining (MSCG) method developed by Voth and co-workers.<sup>18–22</sup> This approach does not only preserve statics and dynamics during the mapping procedure, it also allows to include additional physical constraints during the fitting procedure, and allows to proceed beyond the pair potential level.<sup>21</sup>

In what follows, we provide a short description of the employed MSCG approach. We distinguish between quantities in the MR and CG pictures by denoting the corresponding properties with lower- and upper-case symbols, respectively. Each dendrimer was mapped to a single interaction site, which was located at the center-of-mass (CM) of the original macromolecule,

$$\mathbf{r}_{\text{CM},I} = \mathbf{R}_I = \frac{1}{n_m} \sum_{i=1}^{n_m} \mathbf{r}_i, \quad (4)$$

where  $\mathbf{r}_i$  denotes the position of monomer  $i$  of the  $I$ th dendrimer (omitting in the following the index  $I$  for clarity). The size of the coarse-grained particle was defined through the dendrimer's radius of gyration,

$$R_g^2 = \frac{1}{n_m - 1} \sum_{i=1}^{n_m} (\mathbf{r}_i - \mathbf{r}_{\text{CM},I})^2. \quad (5)$$

We assumed that the effective interaction between the CG particles depended only on the interparticle distance and that all interactions were pairwise additive. Furthermore, we introduced a cutoff radius,  $R_{\text{max}}$ , beyond which CG particles did not interact with each other. In the MSCG framework, the force acting on the effective particle  $I$ ,  $\mathbf{F}_I(\mathbf{R}^N)$ , is given by

$$\mathbf{F}_I(\mathbf{R}^N) = \sum_{J=1, J \neq I}^N f(R_{IJ}) \hat{\mathbf{R}}_{IJ}. \quad (6)$$

Here,  $\mathbf{R}^N$  represents the entire set of the  $\mathbf{R}_I$  (with  $I = 1, \dots, N$ ),  $R_{IJ} = |\mathbf{R}_{IJ}| = |\mathbf{R}_J - \mathbf{R}_I|$  is the distance between particles  $I$  and  $J$ , and  $\hat{\mathbf{R}}_{IJ}$  denotes the unit vector pointing along  $\mathbf{R}_{IJ}$ .

The function  $f(R)$  in Eq. (6) is non-zero in the range  $0 \leq R \leq R_{\text{max}}$  and needs to be determined from the MR simulations. For the explicit evaluation of  $f(R)$ , we divided the interval  $[0, R_{\text{max}}]$  into  $N_D$  equally spaced sub-intervals and performed a piecewise decomposition of  $f(R)$  into a sum over basis-functions,  $f_d(R)$ ,

$$f(R) = \sum_{d=0}^{N_D} \phi_d f_d(R), \quad (7)$$

where  $f_d(R)$  are linear splines with yet unknown coefficients  $\phi_d$ . The functional form of a spline in the interval  $[R_{d-1}, R_{d+1}]$  is given by

$$f_d(R) \equiv \begin{cases} \frac{R - R_{d-1}}{R_d - R_{d-1}} & \text{if } R_{d-1} < R \leq R_d \\ \frac{R_{d+1} - R}{R_{d+1} - R_d} & \text{if } R_d < R \leq R_{d+1} \\ 0 & \text{otherwise.} \end{cases} \quad (8)$$

The actual values of  $N_D$  and  $R_{\text{max}}$  are system-specific and will be reported in the corresponding Subsections III A–III C, where the respective results are presented and discussed.

The effective potentials for the CG simulations were then calculated by determining the coefficients  $\phi_d$  in Eq. (7) from MR simulations conducted at the exact same density. Substituting  $\mathbf{R}^N$  and  $\mathbf{F}^N$  by  $\mathbf{r}_{\text{CM}}^N$  and  $\mathbf{f}_{\text{CM}}^N$  led to a set of  $N$  linear equations of the  $N_D$  parameters, which were solved using the least-squares algorithm.<sup>41,42</sup> To improve sampling, the parameters were computed and averaged from  $n_t$  statistically independent configurations. In practice, snapshots were taken for every 500–5 000 time steps, and we carefully checked that the solutions converged by continuously increasing  $n_t$  until the results did not change anymore. We found that 10 000–25 000 configurations were in general sufficient to meet these requirements. We verified the correct implementation of the MSCG algorithm by comparing the effective pair potentials computed

at infinite dilution with previously published data; for example, compare  $\Phi_{\text{eff}}^0$  in Fig. 3 with the data shown in Fig. 4(c) in Ref. 6, which has been computed using Boltzmann inversion.

### III. RESULTS

#### A. Dendrimers in a good solvent

In order to test the MSCG algorithm, we first studied a system of dendrimers in a good solvent. Under these conditions, the macromolecules should not exhibit any clustering but should be distributed homogeneously in the system. In Ref. 23, Götze *et al.* calculated the effective potential of dendrimers ( $G=4$ ,  $p=1$ , and  $f=3$ ) in a good solvent at  $T=1$ . In the limiting case of infinite dilution, i.e., for  $\rho \rightarrow 0$ , an effective potential  $\Phi_{\text{eff}}^0(r)$  with a Gaussian shape was obtained. The transferability of this model was tested by conducting additional MR simulations for densities up to the overlap density and comparing the resulting pair correlation functions  $g(r)$  with the ones obtained from CG simulations using  $\Phi_{\text{eff}}^0(r)$ .<sup>43</sup> Excellent agreement was observed for the entire density range with only slightly higher ordering observed in the MR simulations. This discrepancy was attributed to the deformation of the individual dendrimers in the MR simulations, which was not included in the employed CG model.

In this contribution, we extended the density range upto  $\rho = 2\rho_{\text{overlap}}$  using  $N = 500$  dendrimers. We measured a radius of gyration of  $R_g = 3.41$  for these macromolecules and computed the effective pair interaction using a set of  $N_D = 8$  basis functions and a cutoff radius  $R_{\text{max}} = 20$ . The main panel of Fig. 2 shows a comparison of the CM  $g(r)$ , computed both in the MR and CG simulations. Remarkable agreement between the two datasets is evident, with a slightly more pronounced local structuring in the CG simulations. We do not expect a perfect match between the  $g(r)$  data from the MR and CG simulations, as agreement of these structural properties is not explicitly imposed in the mapping procedure. The quality of the agreement is comparable to previously published results based on the MSCG algorithm for different systems, see, for example, Fig. 1 in Ref. 20 and Fig. 4 in Ref. 21.

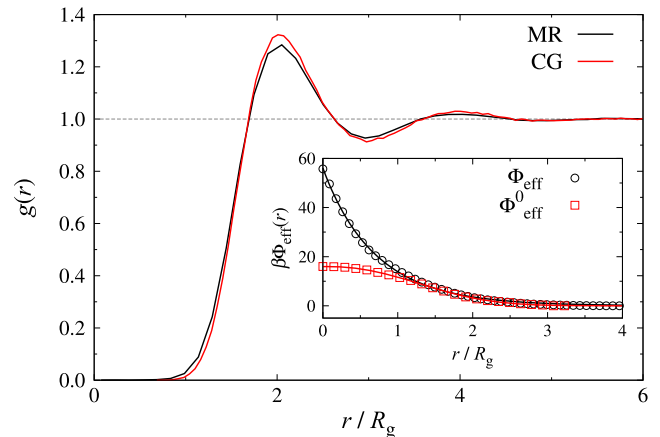


FIG. 2. Comparison of the radial distribution function  $g(r)$  computed both in MR and in CG simulations (as labeled), carried out at  $\rho = 2\rho_{\text{overlap}}$ . The CG simulation has been conducted with an effective pair potential,  $\Phi_{\text{eff}}(r)$ , computed at the same density as the MR simulation;  $\Phi_{\text{eff}}(r)$  is shown in the inset together with its fit to  $\Phi_{\text{GEM}}^n(r)$  with  $n = 0.97$ .

The inset of Fig. 2 shows the corresponding effective potential  $\Phi_{\text{eff}}(r)$  and it is well visible that it changed significantly compared to its form at infinite dilution,  $\Phi_{\text{eff}}^0(r)$ ; as  $\rho$  was increased beyond  $\rho_{\text{overlap}}$ , the effective pair potential became significantly steeper at the origin. This effect can be attributed to the steric interactions between the monomers, which impeded the overlap of nearby dendrimers at high densities.

To obtain a functional form for  $\Phi_{\text{eff}}(r)$ , we fitted the computed potential via the generalized exponential model of index  $n$  (GEM- $n$ ),<sup>5</sup>

$$\Phi_{\text{GEM}}^n(r) = \varepsilon_{\text{GEM}} \exp[-(r/\sigma_{\text{GEM}})^n], \quad (9)$$

where  $\varepsilon_{\text{GEM}}$  parameterizes the strength of the potential,  $\sigma_{\text{GEM}}$  is the diameter of the effective particle, and  $n$  controls the steepness of the shoulder. For  $n = 1$ ,  $\Phi_{\text{GEM}}^1(r)$  decays exponentially, while this function becomes a Gaussian for  $n = 2$ . In the limit of  $n \rightarrow \infty$ ,  $\Phi_{\text{GEM}}^\infty(r)$  becomes a square shoulder potential. It has been demonstrated in Ref. 44 that particles interacting via a  $\Phi_{\text{GEM}}^n(r)$  potential exhibit clustering if  $n > 2$ .

We obtained an exponent of  $n = 0.97$  for the simulations conducted at  $\rho = 2 \rho_{\text{overlap}}$ , whereas  $n = 2$  was found for the situation at infinite dilution. Both values are below the theoretically estimated threshold for clustering, which is in agreement with the expected behavior for these macromolecules dispersed in a good solvent. Hence, these findings confirm that the force-matching algorithm can be used for non-aggregating dendrimers even at densities significantly larger than  $\rho_{\text{overlap}}$ .

## B. Amphiphilic dendrimers—Model I

In order to study the density dependence of the effective potentials in *clustering* systems, we first simulated the amphiphilic dendrimer systems investigated in Ref. 6. These dendrimers had a functionality of  $f = 3$ , a spacer length of  $p = 1$ , and were terminated in their growth after  $G = 2$  generations (see Fig. 1). Mladek *et al.* calculated the zero-density effective potential for these amphiphiles<sup>6</sup> and demonstrated that it fulfills the clustering criterion derived in Ref. 44. Lenz *et al.* attempted to verify the validity of the CG picture at finite densities by performing MR simulations in the fluid state.<sup>11</sup> They found qualitative agreement between the pair correlation functions in the MR and CG simulations (using the zero-density effective potential) at low and intermediate densities.

In order to provide a more quantitative analysis, we systematically computed the effective potentials at five *finite* densities, i.e.,  $\rho = 0.38, 0.52, 0.65, 0.82$ , and  $1.05$ . This density range covers the state points investigated in Ref. 11. We simulated an ensemble of  $N = 2000$  dendrimers for all densities ( $N = 500$  for  $\rho = 0.38$ ) to ensure proper sampling of the measured system properties.

The main panel of Fig. 3 shows all  $\Phi_{\text{eff}}(r)$ , which were computed using the MSCG algorithm with a basis of dimension  $N_D = 13$  and a cutoff radius  $R_{\text{max}} = 20.0$ . The effective potential  $\Phi_{\text{eff}}(r)$  between two isolated amphiphiles ( $\rho \rightarrow 0$ ) has a local minimum at  $r = 0$ , which corresponds to a configuration where the solvophobic cores of the two dendrimers overlap. The effective potential had its maximum at  $r \approx R_g$ , i.e., when the solvophilic shell of a dendrimer penetrates the solvophobic core of another one, and vice versa.

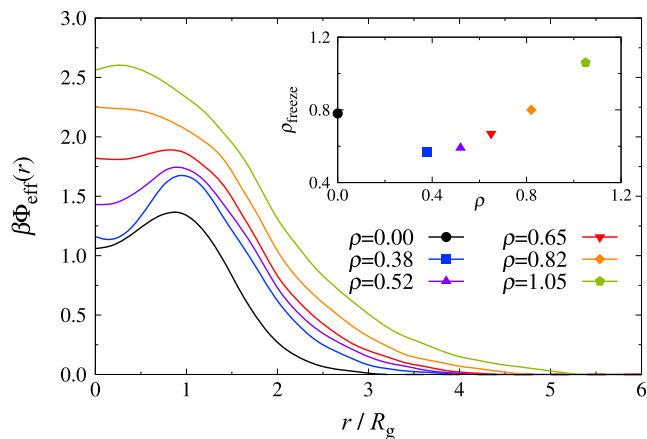


FIG. 3. Effective potential  $\Phi_{\text{eff}}(r)$  of a system of amphiphilic dendrimers (model I) computed at different densities (as labeled). The  $x$ -axis has been scaled by the radius of gyration  $R_g$  at the respective density  $\rho$ . Inset: freezing density calculated from Eq. (10) using the effective pair potential computed at the  $\rho$ -value specified in the  $x$ -axis.

Our analysis revealed a strong density dependence of  $\Phi_{\text{eff}}(r)$ : the long-ranged repulsion of the potential increased monotonically with  $\rho$ , while the short-ranged attraction, characterized by  $\Delta\Phi_{\text{eff}} = \Phi_{\text{eff}}(R_g) - \Phi_{\text{eff}}(0)$ , gradually disappeared. However, we found an intermediate density range  $0 < \rho < 0.52$ , where  $\Delta\Phi_{\text{eff}}$  increased, indicating an enhanced affinity to form clusters.

The state point at which the system freezes into a cluster crystal can be estimated accurately by minimizing the free energy of the crystal with respect to the cluster occupation number and lattice spacing.<sup>5,45</sup> Following the arguments brought forward in Ref. 45, the freezing density,  $\rho_{\text{freeze}}$ , can be calculated directly from the effective potential  $\Phi_{\text{eff}}(r)$  through

$$\frac{T_{\text{freeze}}}{\rho_{\text{freeze}}} \approx 1.393 \left| \tilde{\Phi}_{\text{eff}}(k_{\text{min}}) \right|, \quad (10)$$

where  $T_{\text{freeze}}$  is the freezing temperature,  $\tilde{\Phi}_{\text{eff}}(k)$  is the Fourier transformation of  $\Phi_{\text{eff}}(r)$ , and  $k_{\text{min}}$  is the position of the minimum of  $\tilde{\Phi}_{\text{eff}}(k)$ . One peculiar property of Eq. (10) is the constant ratio between  $T_{\text{freeze}}$  and  $\rho_{\text{freeze}}$ , which leads to a straight freezing line in the  $(T, \rho)$ -phase diagram.<sup>45</sup>

We computed  $\rho_{\text{freeze}}$  for each  $\Phi_{\text{eff}}(r)$  at a fixed freezing temperature  $T_{\text{freeze}} = T = 1$  and plotted the data in the inset of Fig. 3. Here, we can see that  $\rho_{\text{freeze}}$  changed significantly as  $\rho$  was increased: for  $\rho \leq 0.65$ ,  $\rho_{\text{freeze}}$  decreased with respect to the freezing density in the zero-density limit,  $\rho_{\text{freeze}}^0$ . In fact,  $\rho_{\text{freeze}}$  attained its minimum at  $\rho = 0.38$ , the same density where  $\Delta\Phi_{\text{eff}}$  is maximized. These data suggest that, initially, clustering was enhanced by the presence of additional amphiphiles. At low densities, it was beneficial to place dendrimers on top of each other, since this strategy decreased the contact area of the solvophobic cores with the surrounding solvent. However, as the density was increased further, excluded volume effects made it increasingly difficult to place additional dendrimers into a cluster. This interpretation is supported by the slight swelling of the dendrimers, quantified via the increase of  $R_g$  from  $R_g = 3.30$  to  $R_g = 3.36$  (measurement uncertainty  $\pm 0.01$ ) as the density was increased.

Figure 4 shows the cluster size distribution in the MR simulations, obtained by applying a simple distance-based cluster

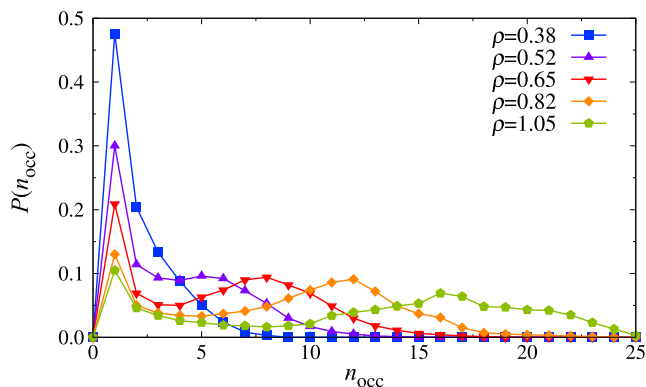


FIG. 4. Probability  $P(n_{\text{occ}})$  to find an amphiphilic dendrimer in a cluster with  $n_{\text{occ}}$  members in the MR simulations of model I at different densities  $\rho$  (as labeled).

analysis algorithm, where dendrimers with a CM separation of less than  $r_c = 0.9 R_g$  were assigned to the same cluster. For  $\rho = 0.38$ , approximately half of all dendrimers were isolated and  $P(n_{\text{occ}})$  decreased monotonically with  $n_{\text{occ}}$ . For  $\rho = 0.52$ , the number of isolated dendrimers decreased to  $P(1) = 30\%$ , and we found a local maximum of  $P(n_{\text{occ}})$  at  $n_{\text{occ}} = 6$ , indicating the onset of clustering. As  $\rho$  was increased further,  $P(1)$  kept decreasing while the local maximum of  $P(n_{\text{occ}})$  shifted towards higher values of  $n_{\text{occ}}$ .

We then compared the resulting radial distribution functions  $g(r)$  of the MR simulations with the ones from the CG simulations using  $\Phi_{\text{eff}}(r)$  and  $\Phi_{\text{eff}}^0(r)$ . It is evident from Fig. 5 that the CG simulations using  $\Phi_{\text{eff}}^0$  failed completely in reproducing the structures observed in the MR simulations even at the lowest investigated density ( $\rho = 0.38$ ). In contrast, the agreement between the MR simulations and the CG calculations with  $\Phi_{\text{eff}}(r)$  was significantly better up to  $\rho \leq 0.52$ , but then worsened rapidly as the density was further increased.

In order to better understand the origin of this startling discrepancy, we computed the effective interaction between a single amphiphile and a single cluster of these macromolecules in an otherwise empty simulation box for various occupation numbers  $n_{\text{occ}}$ . Figure 6 shows  $\Phi_{\text{DC}}(r)/n_{\text{occ}}$ , i.e., the effective dendrimer-cluster potential normalized by the occupation number. These data show that  $\Phi_{\text{DC}}(r)$  became increasingly repulsive with increasing  $n_{\text{occ}}$ , a trend which stemmed from crowding effects in the cluster center. However, for sufficiently small  $n_{\text{occ}}$ ,  $\Phi_{\text{DC}}(r)$  was almost linearly additive with respect to  $n_{\text{occ}}$ .

We quantified the additivity of the potentials via

$$\delta = \int_0^{R_{\text{max}}} |\Phi_{\text{eff}}^0(r) - \Phi_{\text{DC}}(r)/n_{\text{occ}}| dr. \quad (11)$$

Figure 7 shows  $\delta$  as a function of  $n_{\text{occ}}$ , and it is clearly visible that  $\delta$  increased with  $n_{\text{occ}}$ . Hence, the description using  $\Phi_{\text{eff}}^0(r)$  worsened with increasing  $n_{\text{occ}}$ , resulting in erroneous structures in the CG description.

In order to understand the failure of  $\Phi_{\text{eff}}$ , it is insightful to consider the cluster distribution  $P(n_{\text{occ}})$  shown in Fig. 4. It becomes immediately clear that the interactions in the system cannot be described through a *single* effective pair potential  $\Phi_{\text{eff}}$ : at high densities,  $P(n_{\text{occ}})$  was rather broad, resulting in a large number of different dendrimer-cluster and cluster-cluster

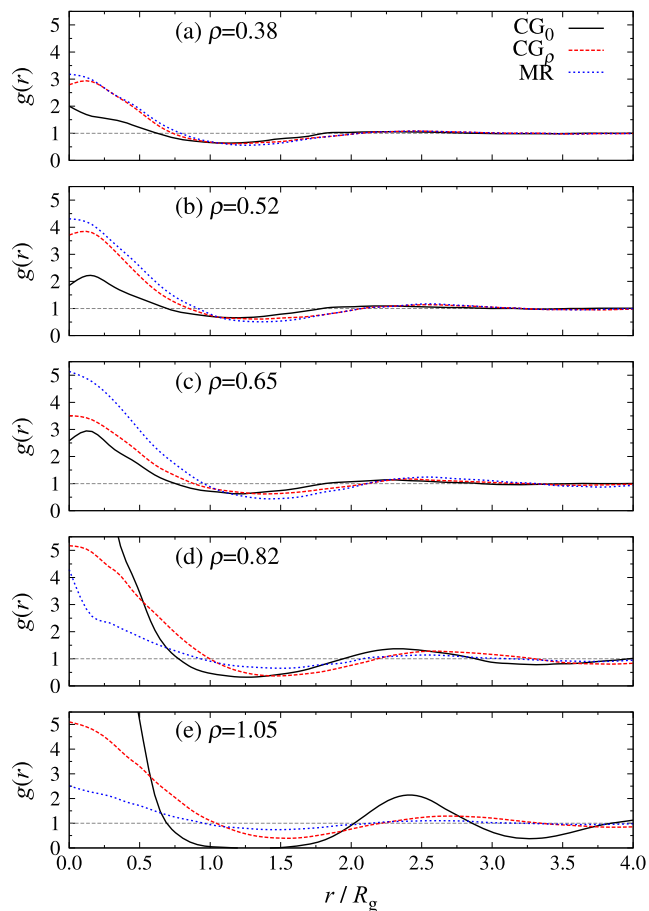


FIG. 5. Comparison of the radial distribution function  $g(r)$  computed in a MR simulation (dotted line), a CG simulation using the potential computed at the corresponding density (dashed line), and a CG simulation using the effective potential computed at infinite dilution (solid line) in a system of amphiphilic dendrimers (model I).

interactions. By mapping all these effective potentials onto a single  $\Phi_{\text{eff}}(r)$ , we only preserve  $\langle n_{\text{occ}} \rangle$  but lose all information concerning the shape of  $P(n_{\text{occ}})$ . This argument is corroborated by the fact that the  $g(r)$  obtained from the MR and CG simulations agreed remarkably well for low density states  $\rho \leq 0.52$ , where the cluster distributions were rather narrow (cf. Fig. 4).

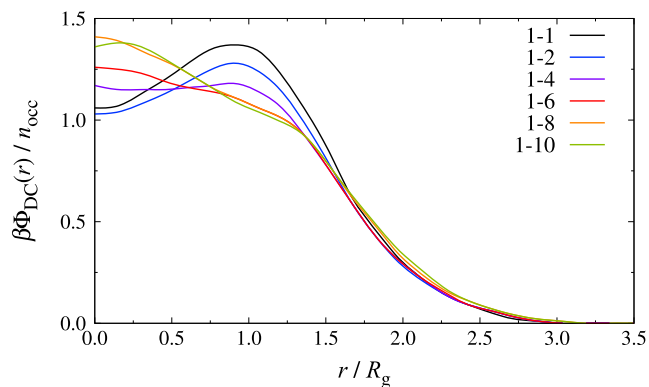


FIG. 6. Normalized effective potential  $\Phi_{\text{DC}}(r)$  between a single dendrimer and a cluster of  $n_{\text{occ}} = 2-10$  dendrimers (model I), computed in a MR simulation. The x-axis has been scaled by the radius of gyration of the amphiphile in the zero density limit,  $R_g$ , and the y-axis has been normalized by the aggregation number  $n_{\text{occ}}$ .

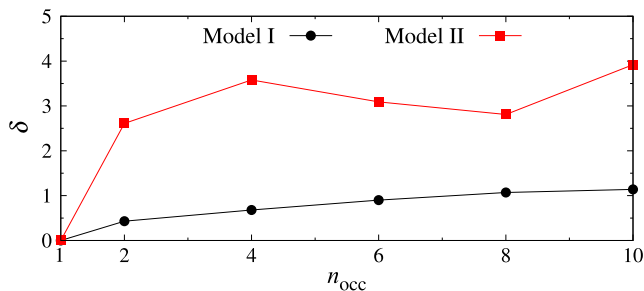


FIG. 7. Deviation  $\delta$  between the reduced dendrimer-cluster potential,  $\Phi_{\text{DC}}/n_{\text{occ}}$ , and the effective dendrimer-dendrimer potential in the zero-density limit,  $\Phi_{\text{eff}}^0$ , as defined through Eq. (11). Data shown for amphiphilic dendrimers of models I and II.

### C. Amphiphilic dendrimers—Model II

To induce clustering of the amphiphiles at lower densities, considerable effort was put into tuning the interaction parameters of model I.<sup>12</sup> In the revised model II, the amphiphiles had a significantly more open core region, which was achieved by increasing the rest length of the central  $g = 0$  bonds. In addition, the range of the attraction between the core monomers was increased and thus acted well beyond the polymer's radius of gyration ( $R_g \approx 3.47 \pm 0.02$  for all investigated densities). These features successfully lowered the freezing density from  $\rho_{\text{freeze}}^0 = 0.78$  (model I) to  $\rho_{\text{freeze}}^0 = 0.141$ . At this point we would like to mention that an erroneous value of  $\rho_{\text{freeze}}^0 = 0.281$  was reported originally in Ref. 12 for the model II due to a miscalculation of the corresponding effective potential  $\Phi_{\text{eff}}^0(r)$ .

We computed  $\Phi_{\text{eff}}(r)$  in the zero-density limit and at the reduced densities  $\rho = 0.033, 0.065, 0.084, 0.099$ , and  $0.115$ , where each system consisted of at least  $N = 1280$  dendrimers. We employed a basis of dimension  $N_{\text{D}} = 20$  and a cutoff radius  $R_{\text{max}} = 20.0$ . The effective potentials  $\Phi_{\text{eff}}(r)$  are plotted in Fig. 8 for all investigated  $\rho$  values. Only a very weak density-dependence of the effective potentials is discernible in this density regime. The inset of Fig. 8 shows the corresponding freezing densities  $\rho_{\text{freeze}}$ , which were consistently lower than the  $\rho_{\text{freeze}}^0$  value.

Figure 9 shows the cluster size distributions  $P(n_{\text{occ}})$  in the MR simulations, where we assigned dendrimers within a distance of  $0.85 R_g$  to the same cluster. As  $\rho$  was increased,

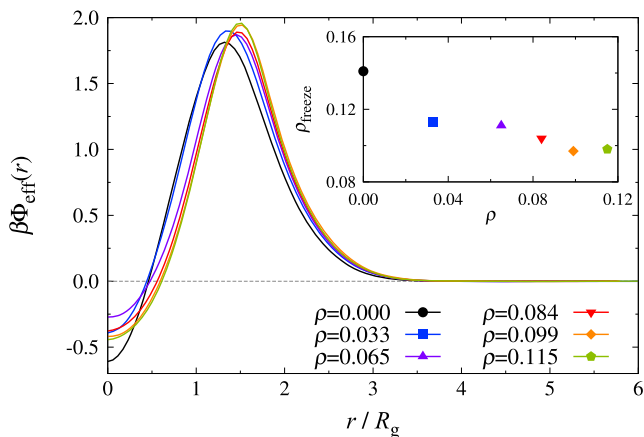


FIG. 8. Same as Fig. 3, but for model II.

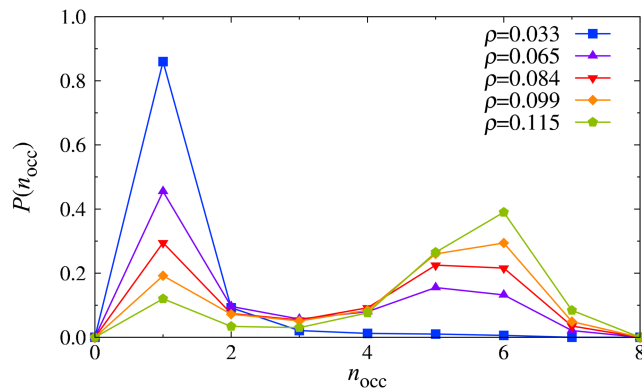


FIG. 9. Same as Fig. 4, but for model II.

the number of isolated amphiphiles decreased continuously and the dendrimers aggregated into clusters. At the same time, the local maximum at  $n_{\text{occ}} > 1$  became more pronounced and shifted towards larger  $n_{\text{occ}}$ . The density at which clustering occurred was considerably lower compared to the model I case, resulting in lower occupation numbers  $n_{\text{occ}}$  (cf. Fig. 4).

At a first glance, the data presented in Figs. 8 and 9 seem to suggest that a CG description using  $\Phi_{\text{eff}}(r)$  should produce good agreement with the MR simulations, since there was only a weak density-dependence on  $\Phi_{\text{eff}}(r)$  and the system had a rather narrow cluster distribution. However, both  $\Phi_{\text{eff}}^0(r)$  and  $\Phi_{\text{eff}}(r)$  failed to replicate the structures of the MR simulations,

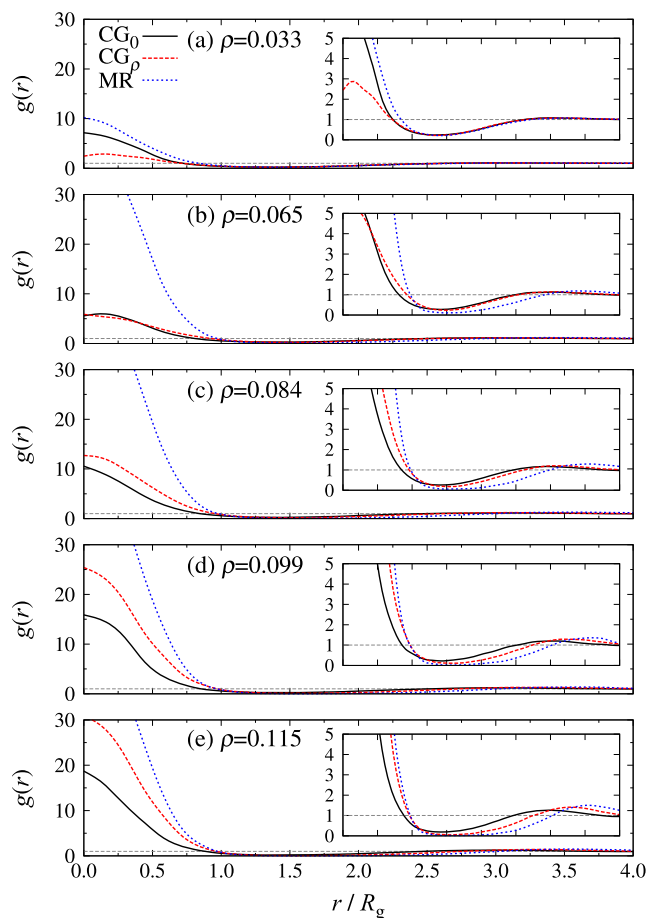


FIG. 10. Same as Fig. 5, but for model II. The inset shows  $g(r)$  with a zoomed in scale on the y-axis.

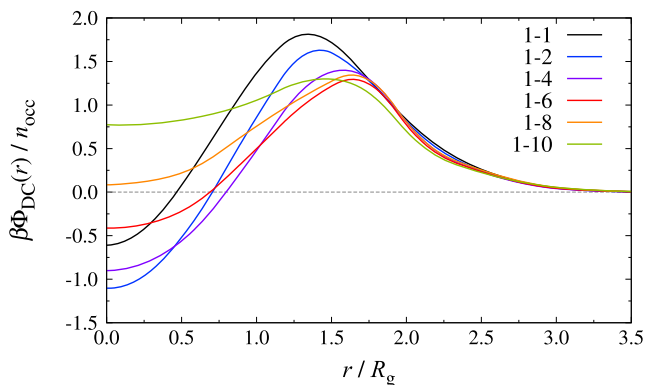


FIG. 11. Same as Fig. 6, but for model II.

as evidenced by the radial distribution functions  $g(r)$  plotted in Fig. 10. In fact, the difference between the MR and CG simulations was significantly more pronounced compared to the model I case investigated in Section III B.

To elucidate this surprising behavior, we computed  $\Phi_{DC}(r)$  for various occupation numbers  $n_{occ}$ , analogous to our previous study of amphiphiles of model I (see Fig. 6). Figure 11 shows the resulting effective potentials, and we can see that the local minimum at  $r = 0$  first decreased but then increased rapidly as  $n_{occ}$  was increased. At the same time, the local maximum monotonically decreased and moved to slightly higher  $r$  values.

Figure 7 shows the deviation of  $\Phi_{DC}/n_{occ}$  [as defined by Eq. (11)] with respect to the effective dendrimer-dendrimer potential in the zero-density limit,  $\Phi_{eff}^0(r)$ . It is clearly visible that the deviations were significantly larger for the model II amphiphiles compared to the ones computed for model I, which explains the inferior agreement of  $g(r)$  shown in Fig. 10.

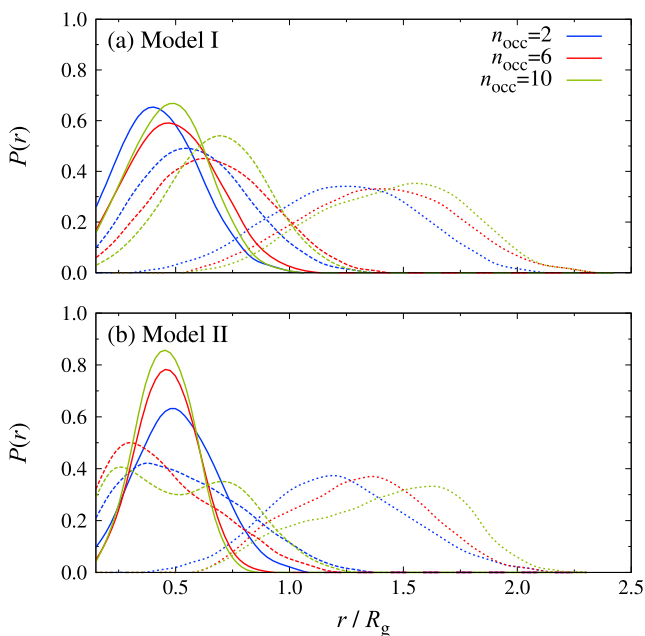


FIG. 12. Probability to find a monomer of generation  $g$  at a given distance  $r$  in a cluster with  $n_{occ}$  amphiphilic dendrimers. The solid lines correspond to the solvophobic  $g = 0$  monomers, the dashed lines to the solvophobic  $g = 1$  monomers, and the dotted lines to the solvophilic  $g = 2$  monomers.

In order to investigate a possible correlation between the conformation of the aggregated dendrimers and  $\Phi_{DC}(r)$ , we measured the radial density distribution of the solvophobic core and solvophilic shell monomers, which is shown in Fig. 12 for selected occupation numbers  $n_{occ}$ . For the model I amphiphiles, we observed a layered structure with the solvophobic  $g = 0$  monomers in the core, the solvophobic  $g = 1$  monomers in the intermediate region, and the solvophilic  $g = 2$  monomers in the shell. In contrast, for the model II amphiphiles, we observed a peculiar backfolding of the  $g = 1$  monomers into the core region, while the  $g = 2$  monomers formed the corona. In general, we observed that the core-shell structure became more pronounced as the cluster occupation number was increased. Furthermore, the conformation of the individual amphiphiles changed only slightly for the investigated values of  $n_{occ}$ , suggesting that the pronounced variation of  $\Phi_{DC}(r)$  predominantly originated from excluded volume effects, which impeded the stacking of dendrimers.

#### IV. CONCLUSIONS

We have calculated effective pair potentials for dendritic polymers at finite densities via a force-matching algorithm and have systematically compared the emerging structural properties in the microscopically resolved and coarse-grained simulations based on effective pair potentials. For non-clustering systems, we observed almost perfect agreement between the two representations, even at densities well above the overlap density. However, a significant mismatch was observed for cluster-forming amphiphilic systems. This was surprising, since we employed effective pair potentials which were computed from the microscopically resolved simulations at exactly the same temperatures and densities.

The reason for this discrepancy is rooted in the heterogeneous density distributions of the clustering systems, which the employed force-matching algorithm is not able to grasp properly. By taking the average over the whole system during the coarse-graining procedure, all information on these cluster distributions is lost. Such an approach becomes problematic when the cluster sizes are not uniformly distributed, and the dendrimer-cluster and cluster-cluster interactions depend on the aggregation number of the partaking clusters.

Hence, improved (or alternative) strategies are necessary for coarse-graining these clustering systems. For instance, it is conceivable to use a set of effective pair potentials, which take into account the local particle density around each interaction site. Such approaches have been suggested for colloidal systems by Rutledge *et al.*<sup>46,47</sup> and Sanyal and Shell<sup>48</sup> for developing implicit solvent models of mixtures and chains, where the effective pair potentials have been determined from fully resolved simulations over a range of global densities and through entropy minimization,<sup>49</sup> respectively. However, the first route is impossible for our clustering systems due to the inherent spatial heterogeneity observed here (see, for example, Fig. 4). The route proposed by Shell *et al.* seems more promising, although transferability to our system might still be an issue as all information is sampled from a single state point. Furthermore, the inclusion of local density fluctuations makes CG simulations considerably more expensive from a

computational view, since they require a complete cluster analysis at each time step. Therefore, further research and/or development of appropriate schemes is required to improve both the accuracy and efficiency of such coarse-grained descriptions.

## ACKNOWLEDGMENTS

This work has been supported by the Marie Curie ITN-COMPLOIDS (Grant Agreement No. 234810), by the Austrian Science Fund (FWF) under Project Nos. P23910-N16 and F41 (SFB ViCoM), and by the WK “Computational Materials Science” of the Vienna University of Technology. Computing time on the Vienna Scientific Cluster (VSC) is gratefully acknowledged. A.N. acknowledges funding from the German Research Foundation (DFG) under the Project No. NI 1487/2-1.

- <sup>1</sup>J. N. Israelachvili, *Intermolecular and Surface Forces*, 2nd ed. (Academic Press, London, 1992).
- <sup>2</sup>K. Kataoka, A. Harada, and Y. Nagasaki, *Adv. Drug Delivery Rev.* **47**, 113 (2001).
- <sup>3</sup>A. Patist, J. R. Kanicky, P. K. Shukla, and D. O. Shah, *J. Colloid Interface Sci.* **245**, 1 (2002).
- <sup>4</sup>L. L. Schramm, E. N. Stasiuk, and D. G. Marangoni, *Annu. Rep. Prog. Chem., Sect. C: Phys. Chem.* **99**, 3 (2003).
- <sup>5</sup>B. M. Mladek, D. Gottwald, G. Kahl, M. Neumann, and C. N. Likos, *Phys. Rev. Lett.* **96**, 045701 (2006); **97**, 019901 (2006).
- <sup>6</sup>B. M. Mladek, G. Kahl, and C. N. Likos, *Phys. Rev. Lett.* **100**, 028301 (2008).
- <sup>7</sup>A. J. Moreno and C. N. Likos, *Phys. Rev. Lett.* **99**, 107801 (2007).
- <sup>8</sup>K. Zhang, P. Charbonneau, and B. M. Mladek, *Phys. Rev. Lett.* **105**, 245701 (2010).
- <sup>9</sup>M. Camargo, A. J. Moreno, and C. N. Likos, *J. Stat. Mech.: Theory Exp.* **2010**(10), P10015.
- <sup>10</sup>N. B. Wilding and P. Sollich, *J. Chem. Phys.* **141**, 094903 (2014).
- <sup>11</sup>D. A. Lenz, B. M. Mladek, C. N. Likos, G. Kahl, and R. Blaak, *J. Phys. Chem. B* **115**, 7218 (2011).
- <sup>12</sup>D. A. Lenz, R. Blaak, C. N. Likos, and B. M. Mladek, *Phys. Rev. Lett.* **109**, 228301 (2012).
- <sup>13</sup>D. Coslovich, L. Strauss, and G. Kahl, *Soft Matter* **7**, 2127 (2011).
- <sup>14</sup>M. Montes-Saralegui, A. Nikoubashman, and G. Kahl, *J. Phys.: Condens. Matter* **25**, 195101 (2013).
- <sup>15</sup>M. Montes-Saralegui, A. Nikoubashman, and G. Kahl, *J. Chem. Phys.* **141**, 124908 (2014).
- <sup>16</sup>A. A. Louis, *J. Phys.: Condens. Matter* **14**, 9187 (2002).
- <sup>17</sup>P. G. Bolhuis, A. A. Louis, J. P. Hansen, and E. J. Meijer, *J. Chem. Phys.* **114**, 4296 (2001).
- <sup>18</sup>S. Izvekov and G. A. Voth, *J. Phys. Chem. B* **109**, 2469 (2005).
- <sup>19</sup>S. Izvekov and G. A. Voth, *J. Chem. Phys.* **123**, 134105 (2005).
- <sup>20</sup>W. Noid, J.-W. Chu, G. Ayton, V. Krishna, S. Izvekov, G. A. Voth, A. Das, and H. C. Andersen, *J. Chem. Phys.* **128**, 244114 (2008).
- <sup>21</sup>A. Das and H. C. Andersen, *J. Chem. Phys.* **131**, 034102 (2009).
- <sup>22</sup>S. Izvekov, P. W. Chung, and B. M. Rice, *J. Chem. Phys.* **133**, 064109 (2010).
- <sup>23</sup>I. O. Götzke, H. M. Harreis, and C. N. Likos, *J. Chem. Phys.* **120**, 7761 (2004).
- <sup>24</sup>M. Bishop, M. H. Kalos, and H. L. Frisch, *J. Chem. Phys.* **70**, 1299 (1979).
- <sup>25</sup>P. Welch and M. Muthukumar, *Macromolecules* **31**, 5892 (1998).
- <sup>26</sup>J. D. Weeks, D. Chandler, and H. C. Andersen, *J. Chem. Phys.* **54**, 5237 (1971).
- <sup>27</sup>S. Plimpton, *J. Comput. Phys.* **117**, 1 (1995).
- <sup>28</sup>W. C. Swope, H. C. Andersen, P. H. Berens, and K. R. Wilson, *J. Chem. Phys.* **76**, 637 (1982).
- <sup>29</sup>M. P. Allen and D. J. Tildesley, *Computer Simulation of Liquids* (Oxford University Press, USA, 1989).
- <sup>30</sup>D. Frenkel and B. Smit, *Understanding Molecular Simulation: From Algorithms to Applications* (Academic Press, 2001).
- <sup>31</sup>S. Nosé, *J. Chem. Phys.* **81**, 511 (1984).
- <sup>32</sup>S. Nosé, *Mol. Phys.* **52**, 255 (1984).
- <sup>33</sup>W. G. Hoover, *Phys. Rev. A* **31**, 1695 (1985).
- <sup>34</sup>W. G. Hoover, *Phys. Rev. A* **34**, 2499 (1986).
- <sup>35</sup>H. A. Karimi-Varzaneh, N. F. A. van der Vegt, F. Müller-Plathe, and P. Carbone, *ChemPhysChem* **13**, 3428 (2012).
- <sup>36</sup>D. Reith, M. Pütz, and F. Müller-Plathe, *J. Comput. Chem.* **24**, 1624 (2003).
- <sup>37</sup>G. Milano and F. Müller-Plathe, *J. Phys. Chem. B* **109**, 18609 (2005).
- <sup>38</sup>D. Levesque, J. J. Weis, and L. Reatto, *Phys. Rev. Lett.* **54**, 451 (1985).
- <sup>39</sup>G. Kahl and M. Kristufek, *Phys. Rev. E* **49**, R3568 (1994).
- <sup>40</sup>R. L. Henderson, *Phys. Lett. A* **49**, 197 (1974).
- <sup>41</sup>C. C. Paige and M. A. Saunders, *ACM Trans. Math. Software* **8**(1), 43 (1982).
- <sup>42</sup>C. C. Paige and M. A. Saunders, *ACM Trans. Math. Software* **8**(2), 195 (1982).
- <sup>43</sup>I. O. Götzke and C. N. Likos, *J. Phys.: Condens. Matter* **17**, S1777 (2005).
- <sup>44</sup>C. N. Likos, A. Lang, M. Watzlawek, and H. Löwen, *Phys. Rev. E* **63**, 031206 (2001).
- <sup>45</sup>C. N. Likos, B. M. Mladek, D. Gottwald, and G. Kahl, *J. Chem. Phys.* **126**, 224502 (2007).
- <sup>46</sup>E. C. Allen and G. C. Rutledge, *J. Chem. Phys.* **128**, 154115 (2008).
- <sup>47</sup>E. C. Allen and G. C. Rutledge, *J. Chem. Phys.* **130**, 034904 (2009).
- <sup>48</sup>T. Sanyal and M. S. Shell, *J. Chem. Phys.* **145**, 034109 (2016).
- <sup>49</sup>M. S. Shell, *J. Chem. Phys.* **129**, 144108 (2008).